

Aalborg Universitet

Frequency control using electric vehicles with adaptive latency compensation and variable speed wind turbines using modified virtual inertia controller

Hosseini, Seved Amir

Published in: International Journal of Electrical Power and Energy Systems

DOI (link to publication from Publisher): 10.1016/j.ijepes.2023.109535

Creative Commons License CC BY-NC-ND 4.0

Publication date: 2024

Document Version Publisher's PDF, also known as Version of record

Link to publication from Aalborg University

Citation for published version (APA):

Hosseini, S. A. (2024). Frequency control using electric vehicles with adaptive latency compensation and variable speed wind turbine's using modified virtual inertia controller. International Journal of Electrical Power and Energy Systems, 155(Part B), Article 109535. https://doi.org/10.1016/j.ijepes.2023.109535

General rights

Copyright and moral rights for the publications made accessible in the public portal are retained by the authors and/or other copyright owners and it is a condition of accessing publications that users recognise and abide by the legal requirements associated with these rights.

- Users may download and print one copy of any publication from the public portal for the purpose of private study or research.
 You may not further distribute the material or use it for any profit-making activity or commercial gain
 You may freely distribute the URL identifying the publication in the public portal -

If you believe that this document breaches copyright please contact us at vbn@aub.aau.dk providing details, and we will remove access to the work immediately and investigate your claim.

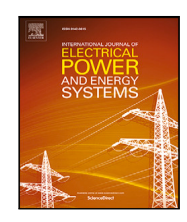
Downloaded from vbn.aau.dk on: November 17, 2025

ELSEVIER

Contents lists available at ScienceDirect

International Journal of Electrical Power and Energy Systems

journal homepage: www.elsevier.com/locate/ijepes





Frequency control using electric vehicles with adaptive latency compensation and variable speed wind turbines using modified virtual inertia controller

Seyed Amir Hosseini

Department of Energy Technology, Aalborg University, 9220 Aalborg, Denmark

ARTICLE INFO

Keywords: Load frequency control Electric vehicle Virtual inertia controller Adaptive latency compensator Variable speed wind turbine

ABSTRACT

In this paper, to reduce the effect of low inertia consequences, electric vehicle (EV) and variable speed wind turbine (VSWT) are adopted to collaborate in the power system frequency regulation. A virtual inertia controller based on the IEC 61851 standard is proposed to benefit from EV contribution in frequency regulation. In this controller, the rate-of-change-of-frequency (ROCOF) is measured and an appropriate EV current set point is obtained. Furthermore, to decrease the effect of frequency regulation on EVs owners, a stochastic allocation method of the regulation sequence among EVs parking lots is presented. One of the barriers of employing EV in the frequency regulation is the communication latency. To overcome this issue, according to the measured latency, a weighted combination of several compensators which is called adaptive latency compensator (ALC) is utilized. After compensating the delay, the output power of the EVs is calculated and collaborated in frequency regulation. In addition, an algorithm is proposed for collaborating VSWT in frequency control. In the proposed algorithm, according to the wind velocity, the output power of the VSWT increases to the maximum acceptable value and will be fixed. A method is developed to find the maximum acceptable increment power considering VSWT constraints. After a supportive part, a recovery part is started to return VSWT hub speed to a desired value. Two PID controllers are designed in this algorithm for support and recovery parts. During the recovery part, a second frequency dip emerges and a method is introduced which at first identifies the second frequency dip moment and EVs collaboration is applied to alleviate this unfavorable outcome. To evaluate the performance of the proposed algorithms and controllers, different simulation studies are conducted using the modified IEEE 39-bus test power system. Results confirm the effectiveness of the proposed methods in system frequency support.

1. Introduction

In recent years, the penetration of renewable energy resources (RESs) like wind and solar in the power system have been increased significantly [1,2]. Wind and solar power plants are converter-connected resources, highly variable and dependent on climate conditions. Therefore, unlike conventional power plants, they are electrically decoupled from the grid [3]. Power system inertia is determined by considering the rotating masses directly connected to the grid [4]. Thus, as adopting RESs increase, the total inertia of the power system decreases. In addition, the high voltage direct current (HVDC) electric power transmission systems have been used recently to transfer power between the interconnected areas [5]. HVDC links separate the inertial response between the interconnected areas. Therefore, the inertial response decreases which makes the power system vulnerable under sudden load changes and generation unit or transmission line outages [6]. As a

result, maintaining the power system frequency in an acceptable range which guarantees a stable and secure operation is more challenging [7]. Variable speed wind turbine (VSWT), demand response (DR), Battery energy storage system (BESS) and electric vehicles (EV) are several state-of-the-art methods to improve the power system frequency regulation [8]. In this paper, EVs and VSWT are employed to collaborate in the frequency regulation.

Excessive consumption of fossil fuels and consequent high air pollution promoted authorities to replace internal combustion engine vehicles with electric vehicles [9]. Significant integration of EVs in the power systems provides a considerable potential of flexible generation and load capability. Furthermore, they act as distributed energy storage systems. Particularly, near 90% of the times, they are plugged into a charging station [10]. Collaboration in load shifting [11], voltage support [12], spinning reserve [13] and frequency regulation [14,15]

E-mail address: Saho@energy.aau.dk.

are several benefits of EVs in the grid. It is worth mentioning that due to some items like circuitry, types and arrangement of EVs' components, various challenges will emerge. Bounded power or energy capacity is one of the challenges that can be solved by employing a lot of EVs [16]. The other one is a relatively long activation time. In other words, there is a latency between sending the control command and changing the output power to a desirable value. This issue is caused due to the signal measurement time, EVs' inverter activation time and communication latency between the central controller and EVs. Signal measurement time and inverter activation time can be omitted by using suitable measurement devices and perfect power electronic tools, respectively. For better performance, the communication latency which varies during time should be compensated somehow.

Collaboration in frequency regulation is one of the interesting EV applications. In [17], based on the power system frequency, a droop control strategy is proposed to adjust the EV charging or discharging power. In [18], a decentralized control procedure is introduced to employ EV in primary frequency control by responding to the system frequency fluctuations. Two optimal real-time strategies based on area control error and area regulation requirements are suggested for EV in [14] to collaborate in the secondary frequency control. An organized charging technique is presented for EV in [19] to improve frequency regulation. In [19], a controller is designed to keep the EV battery state of charge (SOC) around 50%. To adopt EV in frequency adjustment, an optimized fuzzy logic controller is offered in [20] to charge or discharge the EV battery. An optimal controller derived from the sliding mode approach is recommended in [21] to employ EV in secondary frequency control. This controller tries to balance the power generation and load demand of the power system considering the EV.

Nowadays, regarding the environmental concerns, the rate of wind turbine installation and power generation are increased significantly which decreases the power system inertia [22]. Therefore, the stability and operational security of the power system will be jeopardized. One way to decrease this concern is utilizing variable speed wind turbines (VSWT) in the power system frequency and voltage control [23]. VSWTs are categorized in fully rated converters (FRC) and doublyfed induction generators (DFIG) [24]. One of the well-known methods to employ VSWT in the frequency regulation is the power unreserved control. Temporary over-production and inertia control are two main groups of power unreserved control [25,26]. In face of a severe disturbance, the VSWT should increase its output power immediately. It should be noted that every change may not be achievable. This increment leads to hub speed reduction. Based on wind turbine stability, this over-production period is bounded and after that, the hub speed will be recovered. Furthermore, the VSWT will be removed from frequency regulation when the hub speed reaches the minimum acceptable speed.

Wind turbine collaboration in frequency regulation is suggested in some studies. In [27], a strategy about virtual inertia control is presented to emulate inertia and damping properties to enhance frequency regulation. As mentioned in [28], inappropriate tuning of virtual inertia parameters may cause instability in the power system. To have a smoother excursion in front of load increment or generation unit outage, the particle swarm optimization method is applied in [29] to tune the virtual inertia controller parameters. An efficient strategy is presented in [30] to support the frequency via the wind turbine. In this reference, the Hydro-Quebec electricity transmission system suggests an inertia emulation pattern to compensate the power system low inertia effect. In [1], an ancillary frequency controller is implemented in the DFIG wind turbines. The input to state stability concept is employed to set the controller parameters to improve the power system operating conditions. In [31], an inertial controller and a primary frequency response controller are provided in the power system with high penetration of wind turbines. The implemented method can be utilized for power system frequency control during super-synchronous and subsynchronous wind turbine operations. To imitate the inertia response, the stored kinetic energy of the VSWT is employed in [32]. Speed

controller based on fuzzy logic as well as two ancillary controllers are introduced in [33] to boost the frequency response in DFIG based wind turbines.

To fix the issues associated with the previous studies, the main contributions of the present study are as follows:

- A virtual inertia controller based on IEC 61851 standard is presented to employ EVs in the power system frequency regulation. In this controller, the ROCOF of the power system is measured and the corresponding EV output current set point will be calculated. A dead-band is considered in the controller to avoid collaboration of EVs in small ROCOFs. In addition, to follow the technical 1 A granularity EV current change constraint, EV output current oscillation is probable. To avoid this concern, a modification phase is added to the virtual inertia controller. Moreover, a stochastic allocation method of the regulation sequence among EVs parking lots is proposed to reduce the effect of the frequency regulation on customers.
- Applying EV in the power system frequency involves some communication latency. To meet this challenge, an adaptive latency compensator (ALC) is proposed to compensate this variable latency. The ALC consists of some weighted compensators to mitigate the impacts of phase lag due to the latency.
- An algorithm is presented to collaborate VSWT in the power system frequency regulation. After occurring a disturbance, VSWTs can increase their output power for a specific period and then are recovered by a control signal. To achieve this, two PID controllers are designed and their parameters are optimized by genetic algorithm. In addition, according to the wind velocity, the maximum acceptable power increment of the VSWT is obtained. During the recovery stage, a second frequency dip appears, and a method is provided that first identifies the second frequency dip moment and then employs EV cooperation to mitigate this undesirable outcome.
- To evaluate the efficiency of the proposed methods, four simulation scenarios are applied and performed in the modified IEEE 39-bus test power system using MATLAB/SIMULINK. Results confirm the effectiveness of the suggested algorithms.

Note that in the following, Section 2 presents EV framework and its virtual inertia controller. The latency compensation process is reported in Section 3. The frequency regulation algorithm using wind power plants is described in Section 4. The simulation studies and results comparison are given in Sections Sections 5 and 6, respectively. Finally, conclusion section is provided in Section 7.

2. Modeling framework of EV in frequency regulation

2.1. EV virtual inertia controller

Virtual inertia controller is applied to adopt EVs capability in frequency regulation. EV current is controlled with 1 A granularity from 6 A to 16 A according to IEC 61851 standard and EV nominal current is set to 11 A [34]. It should be noted that, this practical restriction can lead to repetitive charging and discharging EV current.

By providing active power which is proportional to the rate of change of frequency (ROCOF), single-phase EV can imitate conventional power plant behavior. EV virtual inertia controller diagram is depicted in Fig. 1. In this figure, the dotted and the solid curves show the ideal and real ROCOF-EV output current droops, respectively. The ROCOF is measured and according to Fig. 1, the current of EV will be obtained. To increase the life span of the EV battery, the EV is prohibited in frequency regulation in front of small ROCOFs. Therefore, a dead band of $(\pm 0.3~{\rm Hz/s})$ is considered in the controller.

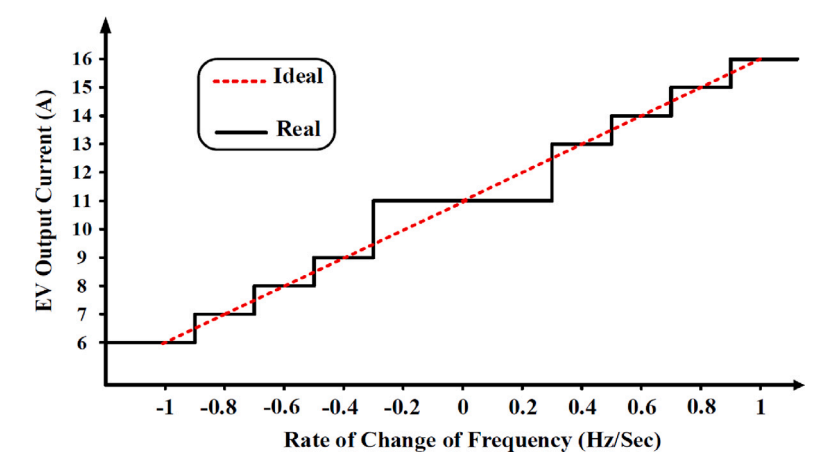


Fig. 1. Virtual inertia controller droop characteristic.

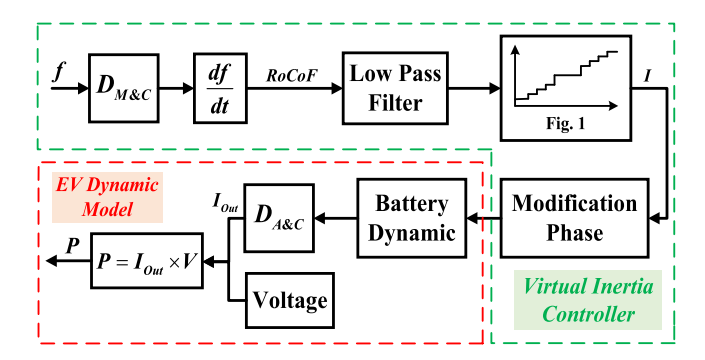


Fig. 2. Virtual inertia controller and EV dynamic model diagram.

2.2. EV participation in frequency regulation

A comprehensive model for participating of EV in frequency regulation is shown in Fig. 2. It consists of, virtual inertia controller and EV dynamic model. In the EV dynamic model part, $D_{A\&C}$ represents the inverter activation and communication latency, V and P are voltage and active power of the EV, respectively. In the virtual inertia control model, f is the frequency of the power system, measured every 200 ms and $D_{M\&C}$ is measurement and communication latency. The modification phase is an algorithm that is demonstrated as follows.

As mentioned, based on IEC 61851 standard, EV current changes in 1 A steps. It can lead to 1 A oscillations. Assume, the output current of the ideal inertia controller is 14.6 A. Therefore, the output current of the real virtual inertia controller will be 15 A. This difference can cause a notable change in the EV output active power. As a result, the difference in active power might alter the power system frequency and ROCOF. Therefore, the output current from the ideal and real virtual inertia controller can be 14.4 A and 14 A, respectively. This movement might repeat several times and can decrease the EV battery life span. As the droop of the virtual inertia controller and the portion of EV in the power system increase, the probability of turning in the loop will be higher.

To overcome this issue, the modification phase is attached to the virtual inertia controller. The control diagram of the modification phase is depicted in Fig. 3. In this diagram, I and I_{Out} are calculated and the output currents of EV, respectively. I'_{Out} is EV output current at the last time step. To consider the charging or discharging status and changed value of the output current, parameter S is introduced. This parameter at the last time step is demonstrated by S'. S has three different values. S=0 is used for controller initialization, S=1 represents that the output current has been increased in the last time step, and S=-1

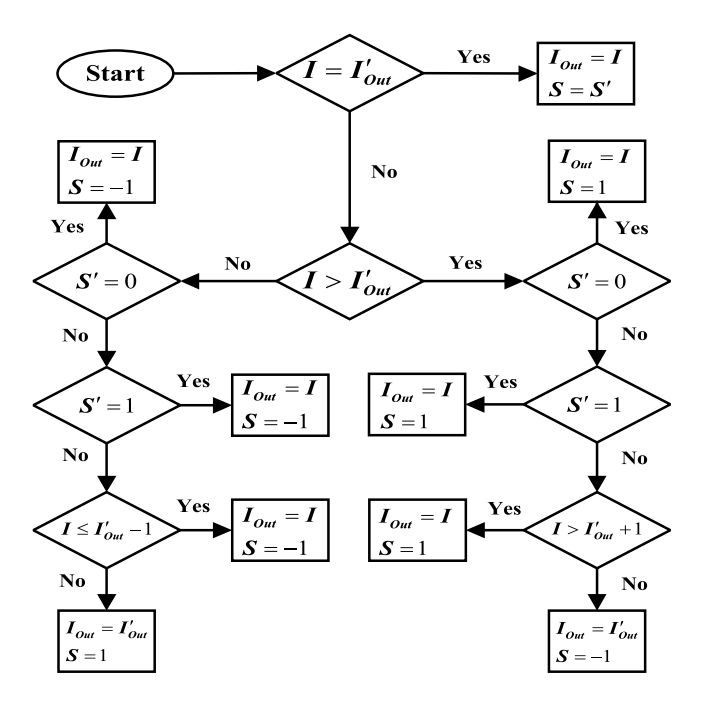


Fig. 3. Modification phase of virtual inertia controller diagram to avoid EV current oscillation.

shows that, the output current has been decreased in the last time step. In the modification phase, I and I'_{Out} are compromised and based on S' value, EV output current oscillation will be avoided.

Since this study aims to investigate the EV's capabilities and limits in providing fast primary control and virtual inertia control, the battery charge state was neglected.

2.3. EVs parking lots participation sequence in power system frequency regulation

Another point that should be mentioned is about different EVs parking lots (EPLs) participation sequences in power system frequency regulation. A threshold value, Δf_T^i , is assigned to the *i*th EPL to collaboratively engage in the frequency regulation. When a certain frequency deviation is reached, the associated EPL begins to participate in the frequency regulation. The first EPL collaborates in the frequency control as soon as the frequency variation in the power system exceeds the minimum frequency violation threshold, Δf_{min} . Furthermore, when the power system frequency deviation exceeds than another threshold,

 Δf_{max} , all EPLs work together to regulate the frequency. The region between these thresholds is divided into a number of potential EPLs and the Δf_T^i for each EPL is obtained. From Δf_{min} to $\Delta f_{min} + \Delta f_T^1$, only the first EPL contributes. From $\Delta f_{min} + \Delta f_T^1$ to $\Delta f_{min} + \Delta f_T^2$, the first and second EPLs collaborate. Because the frequency deviation in the power system is usually greater than Δf_{max} , this process will continue until all EPLs collaborate in frequency regulation. The turn of EPLs collaboration rotates hourly to evenly spread the burden on the EPLs. EPLs with smaller Δf_T participate in the frequency regulating process earlier than others.

3. Communication latency compensation

One of the barriers of using EV in frequency regulation is the communication latency. The communication latency is not fixed due to the communication loads [35]. In the input signals, the communication latency causes phase lag. Thus, an adaptive latency controller (ALC) is required to alleviate the effects of the phase lag. By this compensator, the EV can become an appropriate option for participating in the frequency regulation task.

In the designing process of ALC, the maximum and minimum amounts of latency are required. The proposed ALC consists of a weighted combination of several compensators. The weights are set according to the measured latency. The compensation process is carried out in real-time and the proposed ALC is realized by finite pre-planned compensators. The following equations demonstrate the communication latency compensation algorithm in which " τ " denotes the amount of communication latency. Consider $e^{-\tau s}$ as the transfer function of latency. We have

$$L(s) = e^{-\tau s} = \left(e^{-\frac{\tau}{n}s}\right)^n = \left(\frac{e^{-\frac{\tau}{2n}s}}{e^{\frac{\tau}{2n}s}}\right)^n \simeq \frac{\left(1 - \frac{\tau s}{2n}\right)^n}{\left(1 + \frac{\tau s}{2n}\right)^n}.$$
 (1)

Note that the first-order Pade approximation may cause instability. In other words, a PID controller that stabilizes an approximation may actually destabilize the true system [36]. Although the probability of instability by the first-order Pade approximation decreases as the system order increases, it is recommended that controller parameters should be chosen cautiously.

The phase of L in (1):

$$\Delta L(j\omega) \simeq -2n \times Arctan(\frac{\tau \omega}{2n}),$$
 (2)

Now, a new transfer function that has the same phase lag can be defined as follows:

$$\overline{L}(s) = \frac{1}{(1 + \frac{rs}{2n})^{2n}}.$$
(3)

According to (3), the transfer function associated to each compensator is introduced as below:

$$LC_i(s) = \frac{(1 + \frac{T_i s}{2n})^{2n}}{(1 + T_r s)^{2n}}$$
 for $i = 1, 2, ..., m$. (4)

It should be noted that each mentioned compensator in (4) compensates a certain amount of communication latency. Here, the time constant T_c is a constant parameter which can vary according to the dynamic of the involved system. Notice that the proposed ALC is a weighted combination of mentioned compensators in (4) as follows:

$$ALC(s) = \frac{Num(s)}{Den(s)} = \sum_{i=1}^{m} W_i(\tau) LC_i(s),$$
 (5)

where W_i is the weighting factor associated with the *i*th compensator, i.e., LC_i . It is worth mentioning that the zeros of ALC(s) are selected

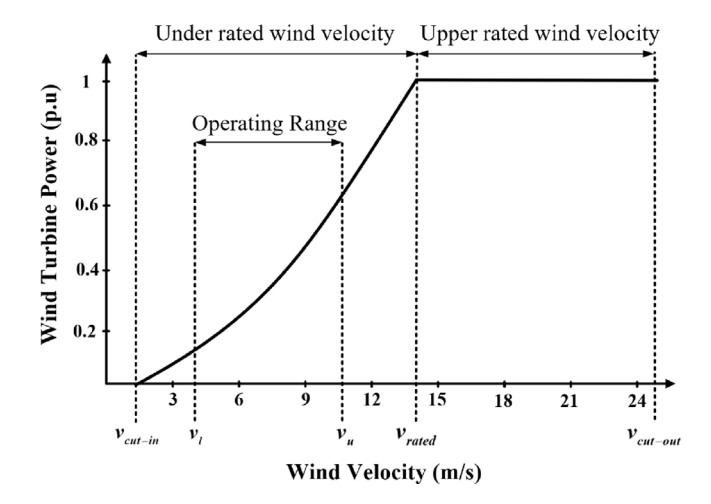


Fig. 4. Electric power of the wind turbine versus wind velocity.

to compensate the phase lag. Therefore, the numerator of (5) should be equal to the denominator of (3). This leads to the following equation:

$$Num(s) = \sum_{i=1}^{m} W_i(\tau) (1 + \frac{T_i s}{2n})^{2n} \equiv (1 + \frac{\tau s}{2n})^{2n}.$$
 (6)

The quality of compensating the latency completely depends on the number of employed compensators. Notice that after a certain number, employing additional compensators does not have a considerable effect on the compensation process. By satisfying (6), the weighting factors can be calculated using the following system of equations:

$$\begin{cases} \sum_{i=1}^{m} W_{i}(\tau) \times T_{i}^{2n} = \tau^{2n}, \\ \sum_{i=1}^{m} W_{i}(\tau) \times T_{i}^{2n-1} = \tau^{2n-1}, \\ \vdots \\ \sum_{i=1}^{m} W_{i}(\tau) \times T_{i} = \tau, \\ \sum_{i=1}^{m} W_{i}(\tau) = 1. \end{cases}$$
(7)

If m=2n+1, the *Cramer* method can be applied to calculate $W_i(\tau)$ s. It is worth noting that T_1 and T_m are the minimum and maximum amounts of latency, respectively, and T_2 to T_{m-1} are some fixed numbers which can be selected between these extreme values.

4. Frequency regulation support from wind farms

4.1. Wind turbine principles

The wind turbine power versus wind velocity curve is sketched in Fig. 4. The wind velocity is categorized into under and upper rated wind velocities. To adjust the power to the rated value in the upper and around rated wind velocities, the pitch controller is activated. At the middle wind velocities, the dynamic of the wind turbine hub is derived by the generator torque control and the aerodynamic torque. Around the left side of the under rated wind velocity, start-up and shut-down modes are triggered.

Furthermore, to extract wind turbine maximum power at each wind velocity, maximum power point tracking (MPPT) mode is suggested and is formulated as follows.

$$P_{gen} = K_{opt}\omega^3. (8)$$

where, the constant, K_{opt} , is obtained as below:

$$K_{opt} = \frac{\rho}{2} \pi R^2 C_p(\lambda^*) \left(\frac{R}{\lambda^*}\right)^3. \tag{9}$$

In (9), λ^* is the desired tip speed ratio which makes the maximum power coefficient.

Changing wind turbine hub speed is necessary to exploit the kinetic energy from the wind turbine. Notice, some changes are not feasible. As shown in Fig. 4, upper and under rated wind velocities are two different power generation methods in the VSWT [37].

Wind turbine single mass model is described as follows:

$$J\frac{d\omega}{dt} = T_{aero} - T_{gen} \tag{10}$$

where, J is the inertia of the wind turbine hub in (kg m²), T_{aero} and T_{gen} are wind turbine aerodynamic and generator torques. T_{aero} is equal to:

$$T_{aero} = \frac{\frac{\rho}{2}\pi R^2 v^3 C_p(\lambda, \beta)}{\omega} \tag{11}$$

The generator torque which is a function of squared hub speed adjusts the wind turbine operating point. At the steady state, desired tip speed ratio, λ^* , is set according to the wind velocity. To produce wind turbine inertia response, ΔT is attached to the generator torque according to the following equation.

$$T_{gen} = K_{opt}\omega^2 + \Delta T. ag{12}$$

Notice, K_{opt} was introduced in (9).

Several controllers have been presented to release inertial response from wind turbines to collaborate in frequency regulation. One of them is power reference term. In this state, the ΔT is:

$$\Delta T = \frac{M}{\omega} \tag{13}$$

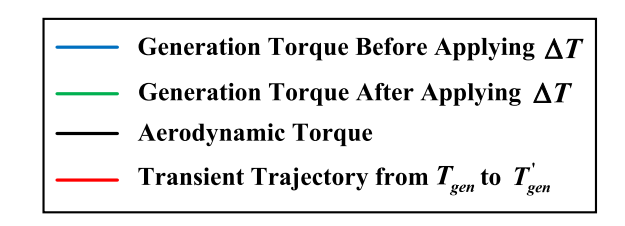
where, M is constant. By adjusting the value of M, this controller changes turbine hub speed. Therefore, the released kinetic energy of the wind turbine changes. The torque curves versus hub speed of the wind turbine are depicted in Fig. 5 where T_{gen} and T'_{gen} are the steady state generator torques of the wind turbine before and after applying ΔT . These torques are described in Eq. (14).

$$\begin{cases} T_{gen} = K_{opl}\omega^2, \\ T'_{gen} = K_{opl}\omega^2 + \frac{M}{\omega}, \end{cases}$$
(14)

As shown in Fig. 5, increasing the generator torque (positive M), leads to hub speed reduction. In addition, the red curve shows the transient trajectory. It should be noted that, to have a stable operation, T'_{gen} should have an intersection with T_{aero} . Furthermore, after increasing the VSWT power, the output power must be lower than maximum output power of the wind turbine and the final hub speed must be upper than minimum hub speed. To find the maximum allowable value for M, an algorithm is proposed in Fig. 6. P_0 is the initial power of VSWT before increasing, P_{max} is VSWT maximum output power and ω_f is the final hub speed after increasing power. In this algorithm, first, it is assumed that M=0 and T_{gen} and T_{gen}^{\prime} curves are intersected. If the updated VSWT output power is lower than P_{max} , and the VSWT hub speed at the intersection point (ω) is greater than the minimum permissible hub speed value (ω_{min}), 0.01 p.u is added to the size of M. T_{gen} and T'_{gen} curves are intersected again and this process is repeated. When no intersection exists between T_{gen} and T'_{gen} curves or the output power of VSWT is higher than P_{max} or ω is lower than (ω_{min}) , the process is terminated, and the new value of M is referred to as the maximum allowable increment in the output power of VSWT.

4.2. Proposed controller scheme

The first idea of the proposed controller is adopted from the Hydro-Quebec inertia requirement for internal emulation from renewable energy sources. The Hydro-Quebec electricity transmission system was the first one that requested wind power plants to collaborate in the frequency regulation [30]. It was stated that the wind power plants with more than 10 MW rated power should be designed somehow to



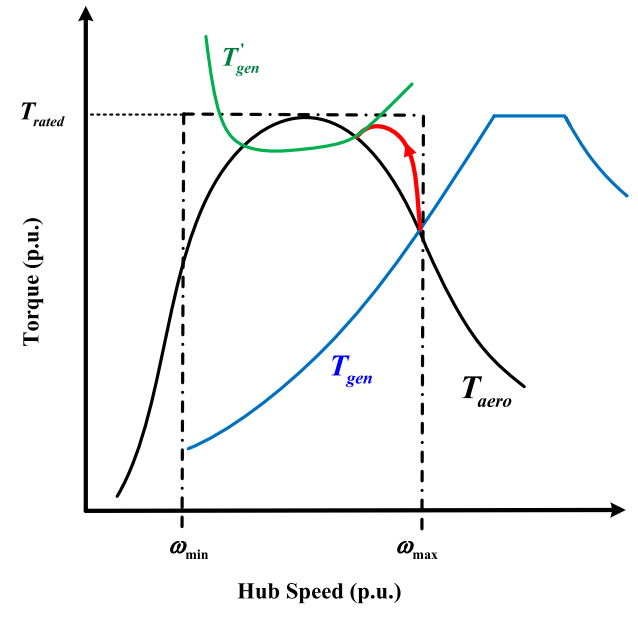


Fig. 5. Aerodynamic, generator and new generator torques and transient response of the VSWT.

Table 1 Hydro-Quebec recommended parameters.

Parameter	Value
Power Increment (PI)	≥6%
Power Decrement (PD)	≤20%
Activation Time (AT)	≤1 (s)
Support Duration (SD)	≥10 (s)
Transition Time (TT)	≥3.5 (s)
Recovery Duration (RD)	≤20 (s)

cooperate in power system frequency control. According to the Hydro-Quebec electricity transmission system suggestion, the wind power plants are employed in frequency control in face of higher than 0.5 Hz and less than 10 s frequency deviations. The proposed strategy is shown in Fig. 7. In this figure, "PI" and "PD" are power increment and power decrement, respectively. Furthermore, "AT", "SD", "TT" and "RD" are activation time, support duration, transition time and recovery duration. Point 1 is the starting point. From point 1 to point 2, the wind turbine reaches maximum participatory power. From Point 2 to point 3 the overproduction power is fixed. Decreasing the additional output power is started from point 3 to point 4. At point 4, the recovery part is started and continues to point 7. The recommended parameters of this approach are presented in Table 1. As seen in the table, the maximum boundary for "PI" and the minimum boundary for "RD" were not reported. In other words, according to the wind turbine dynamic, it might be impossible to increase its power more than 6% and be recovered in less than 20 s. To this end, an algorithm is proposed. The proposed algorithm contains some states which based on the measured frequency and its ROCOF value is activated. Ramping up and uniform support states are controlled by the first PID controller and there is another PID controller for the recovery state.

The structure of the proposed algorithm is demonstrated as below:

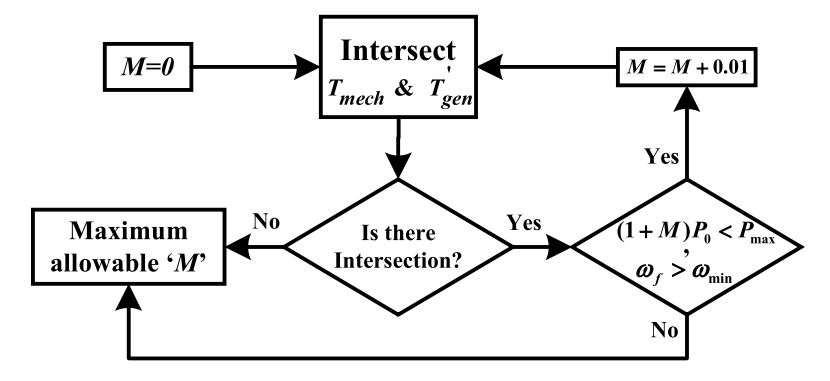


Fig. 6. The proposed algorithm to find the maximum value for M.

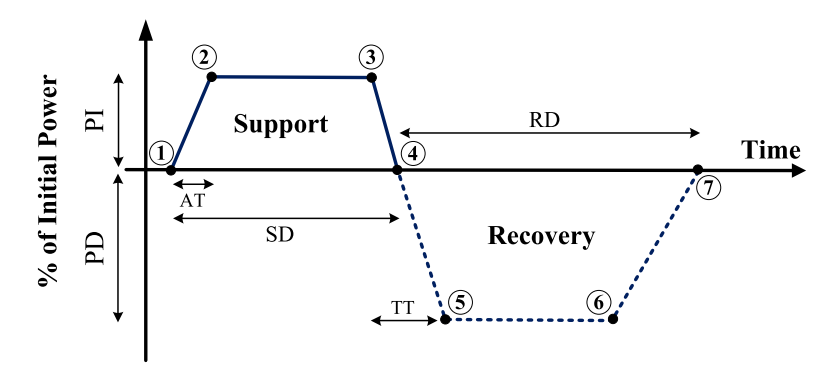


Fig. 7. Hydro-Quebec proposed scheme for VSWT to contribute in frequency regulation.

- Idle state: In this state, the frequency deviation is not enough to request the wind turbine to collaborate in frequency control. Here, by intersecting T_{aero} and T_{gen} curves, the wind turbine hub speed operating point is obtained.
- Activation state: when the frequency is lower than 49.95 Hz and ROCOF is negative, the process is started by considering ΔT from Eqs. (13) and (14) as control signal.
- Ramping up state: the wind turbine output power ramps up in one second. The wind turbine can be more helpful in maintaining frequency in the acceptable range, if its output power is as much as possible. Based on the wind velocity, the maximum allowable value for *M* is obtained from Fig. 6. If the time after activation is lower than one second and the frequency is higher than 49.95 Hz, the turbine stops supporting and transfer to the recovery state. When time is one second and the frequency is not higher than 49.95 Hz, follow the next state.
- Uniform support state: In this state, the increment power will be fixed to the maximum M. The wind turbine operates in this state for a maximum of 10 s or when the wind turbine hub speed, ω , is equal to the minimum acceptable hub speed, ω_{min} . First PID controller is designed to follow ramping up and uniform support states. In this controller, the introduced ΔT in Eq. (13) will be the control signal and is increased in two phases. Therefore, the wind turbine hub speed is reduced according to Fig. 5.
- Recovery state: The final state is the recovery state. In this state, the wind turbine hub speed will be recovered by second PID controller. This controller tries to reduce ΔT to zero. Therefore, the wind turbine hub speed will be set by intersecting the T_{aero} and T_{gen} in a new wind velocity.

The block diagram of the proposed algorithm is shown in Fig. 8, where, USD and AT are uniform support duration and activation time, respectively.

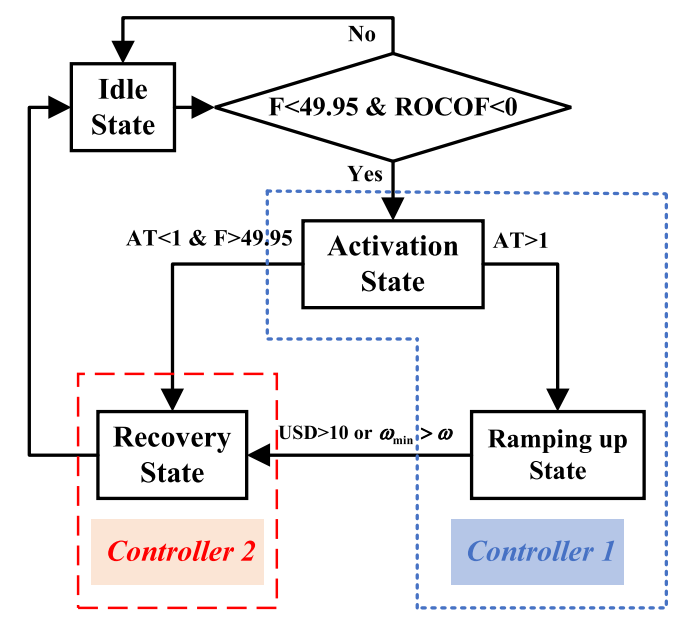


Fig. 8. The proposed algorithm for collaborating VSWT in the frequency regulation.

4.3. Alleviating the second frequency dip

To avoid the second frequency dip, the transition and recovery states of the VSWT should be slow, which can take a considerable time. As this time increases, recovering the power system frequency and the VSWT output power will be unfavorably longer. One solution to decrease the second frequency dip is applying EVs equipped with the adaptive latency controller. The only challenge is then to identify the desired moment to apply the EVs in this process. In other words,

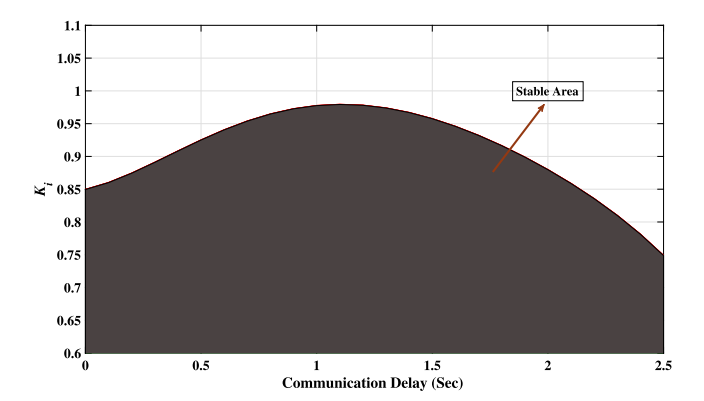


Fig. 9. The stable area based on k_i and τ values.

when the second frequency dip occurs, the EVs controller must be activated. In cases where the VSWT does not participate in power system frequency regulation when the wind velocity increases, the VSWT hub speed ω rises and leads to an increment in the VSWT's output power, P_O , and vice versa. In under-rated wind velocities, the below equation is satisfied:

$$\left(\frac{d\omega}{dt}\right) \times \left(\frac{dP_O}{dt}\right) > 0. \tag{15}$$

When the VSWT collaborates in the frequency regulation, P_O increases and ω decreases during the ramp-up and uniform support states. In the recovery state, however, P_O decreases and ω rises. Accordingly, it can be concluded that when ω rises, $(\frac{d\omega}{dt}) > 0$ and P_O drops $(\frac{dP_O}{dt}) < 0$, the second frequency dip is emerged. Therefore, when both $(\frac{d\omega}{dt}) > 0$ and $(\frac{dP_O}{dt}) < 0$ are met, the EVs controller should be activated to decrease the amount of second frequency dip.

5. Simulation and case studies

To investigate and compare the performance of the proposed controllers and algorithms, some studies and simulations are applied in the modified IEEE 39-bus test power system. The specifications of this power system, EV and wind turbine properties are given in [38]. The performance evaluation contains four scenarios. It should be noticed that, in the scenarios that the EVs collaborate in the frequency regulation, it is supposed that near 15 000 EVs are plugged into a charging spot. In addition, the time constant T_c in ALC is considered 0.05 s. Furthermore, in the scenarios that the wind turbines support the frequency control, around 40% of the power is provided by wind farms. The integral controller parameter in the secondary control loop is adjusted by employing the Genetic Algorithm (GA). As mentioned earlier, the first-order Pade approximation may cause instability. Therefore, this coefficient, k_i , should be tuned to keep the system stable in the face of different communication delay scenarios. It is assumed that the maximum communication delay is not greater than 2.5 s. The shaded area in Fig. 9 illustrates the values of k_i and τ that preserve the system stability. Hence, in order to avoid endangering the stability of this power system, k_i should be lower than 0.75. The objective function of the optimization problem in GA is a weighted summation of the minimum amount of frequency and 1-norm of frequency response.

• Scenario 1: In this scenario, the proposed methods and controllers in Sections 2 and 3 for evaluating EV participation in the power system frequency regulation are utilized. This scenario has three different states and in all of them, at t=5 s, a step load increment $\Delta P_L = 175$ MW is applied in the system as a disturbance. At first state, it is assumed that the power system is just equipped by the droop speed governors plus automatic generation control (AGC). The frequency excursion is shown in Fig. 10 with the solid

green curve. The frequency deviation is high, therefore in the second state, the EV with the proposed virtual inertia controller is added to the power system. The disturbance is applied and the frequency excursion is depicted in Fig. 10 with the dashed blue curve. Employing EV in the power system improves the frequency regulation. Finally, in the third state, the ALC with $\tau=400~{\rm ms}$ is attached to the virtual inertia controller to decrease the effect of communication latency. The frequency excursion of this state is sketched in Fig. 10 with the solid red curve. In comparison to the other states, the frequency deviation is decreased which shows the performance of the EV and ALC.

In addition, the EV currents set points in both second and third states are shown in Fig. 11. When the virtual inertia controller is not equipped with ALC, the current set point is depicted in Fig. 11 with the dashed blue curve. It is decreased to 9 A and then is recovered. The EV current set point in presence of ALC is represented in Fig. 11 with the solid red curve. In this state, the current set point is decreased to 8 A and then is recovered. It can conclude that applying ALC in EV enhances the EV's ability to participate in the frequency regulation.

- Scenario 2: In this scenario, the maximum increment power of the wind turbine for different wind velocities is obtained. To do this, the proposed algorithm in Fig. 6 is adopted. The results are reported in Fig. 12. As seen, when the wind velocity is greater than 10.3 m/s, the maximum increment power is reduced because of the VSWT maximum output power constraint violation.
- **Scenario 3:** In this scenario, the efficiency of the VSWT participation in the power system frequency regulation is assessed. Here, $\Delta P_{I} = 175$ MW step load increment at t = 5 s is applied as a disturbance. In addition, it is assumed that the power system is equipped with the governor and AGC systems. In this scenario, near 40% of the conventional power plants are replaced by wind power plants. Therefore, the inertia of the power system decreases from 3.97 s to 2.47 s. Here, there are three states. The first state includes conventional and wind power plants without any additional controller on the wind turbines. The second state is the first state plus considering the proposed Hydro-Quebec controller for wind turbines. The difference between the second and third scenarios is applying the proposed controller in Section 4.2 instead of Hydro-Quebec controller for the VSWT. After occurring the disturbance, at the first state, the frequency excursion because of low inertia decreases too much and is depicted in Fig. 13 by the solid blue curve. When the Hydro-Quebec proposed controller is added to the VSWT, the frequency response is shown by the solid red curve in Fig. 13. In this state, the nadir frequency improves significantly. As demonstrated in Fig. 14 by the solid red curve, the wind turbine hub speed is reduced in the supporting zone and is returned in the recovery zone. Finally, at the third state, the proposed controller is considered in the VSWT and the frequency pattern is shown by the dashed black curve in Fig. 13. The wind turbine hub speed in this state is depicted in Fig. 14 by the dashed black curve. The nadir and settling time of frequency as well as wind turbine hub speed are improved remarkably compared to the Hydro-Quebec proposed controller which shows the effectiveness of the proposed algorithms.
- Scenario 4: In this scenario, three different states are defined and in all of them at t = 5 s, a step load increment ΔP_L = 175 MW is applied in the system as a disturbance. For the first state, the power system consists of conventional and wind power plants. The frequency excursion is shown in Fig. 15 by the solid green curve. Obviously, the frequency deviation is high and should be improved somehow. Therefore, the proposed controller in Section 4.2 is adopted to improve the frequency stability. In this state, the frequency excursion is shown by the dashed blue curve in Fig. 15. The nadir frequency is made better. In the third state, the nadir frequency can be better by employing EV and ALC

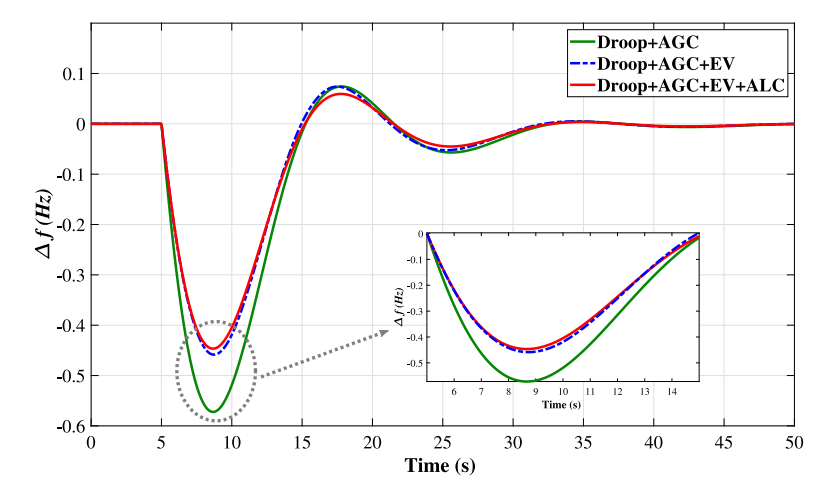


Fig. 10. Power system frequency response with and without participation of EV and ALC.

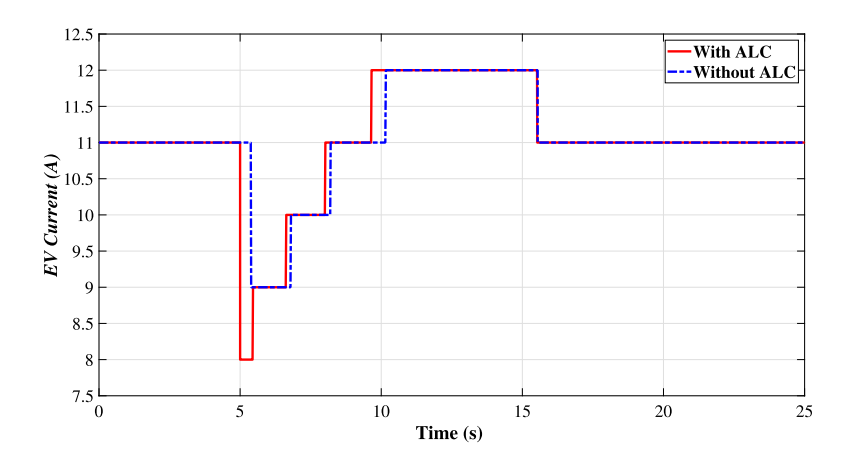
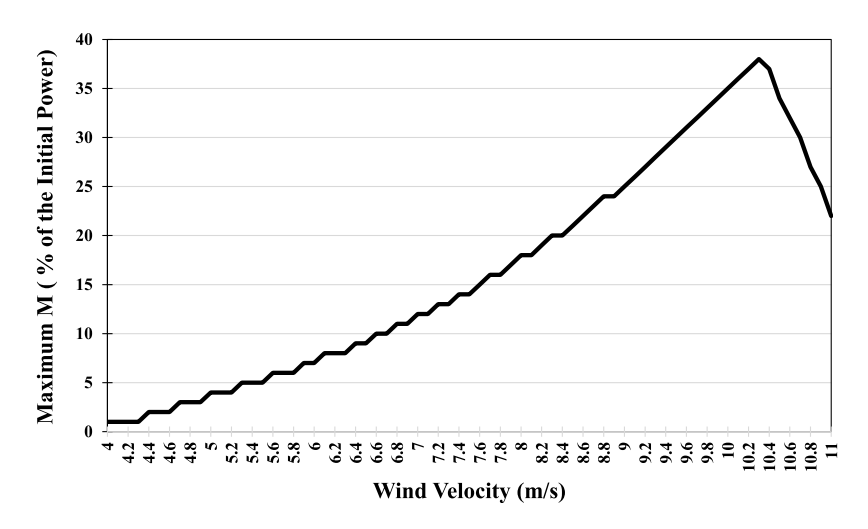


Fig. 11. EV current set point with and without ALC.



 $\textbf{Fig. 12.} \ \ \textbf{Wind velocity versus VSWT maximum increment output power.}$

with $\tau=400$ ms in the frequency regulation as described in Sections 2 and 3. The frequency excursion is shown in Fig. 15 by the solid red curve. In this state with low inertia, the power system frequency regulation improves significantly which shows the effectiveness of the proposed algorithms.

• Scenario 5: This scenario investigates the proposed method in Section 4.3 to find the moment at which the second frequency dip occurs and another group of EVs as well as ALC are applied to

mitigate it. Three different states are considered. In the first state, the VSWT based on the proposed controller in Section 4.2 participates in power system frequency control. The value of the second frequency dip is significant as shown in Fig. 16 with the solid red curve. In the second state, when $(\frac{d\omega}{dt}) > 0$ and $(\frac{dP_O}{dt}) < 0$ are satisfied, the EV controller (with $\tau = 0.5$ s) is applied to the first state to reduce the amount of second frequency dip as depicted in Fig. 16 with the dashed blue curve. As it can be seen, the amount

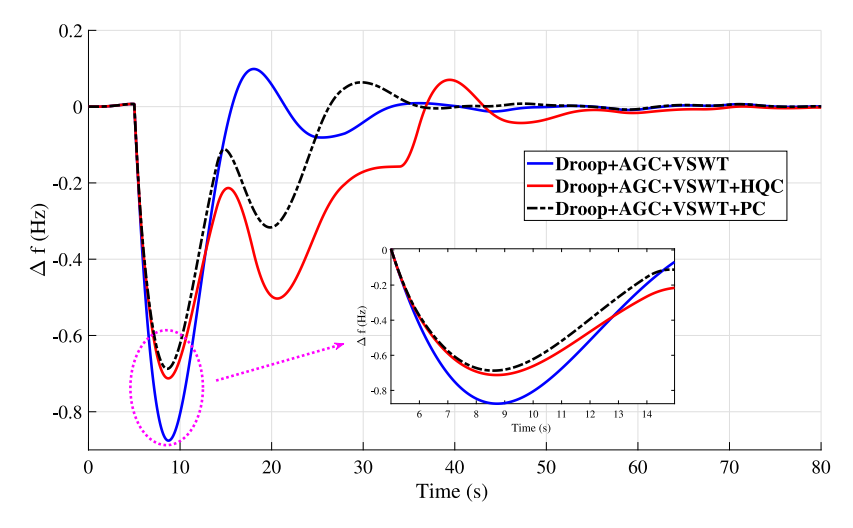


Fig. 13. Power system frequency response considering the VSWT with Hydro-Quebec and the proposed algorithms.

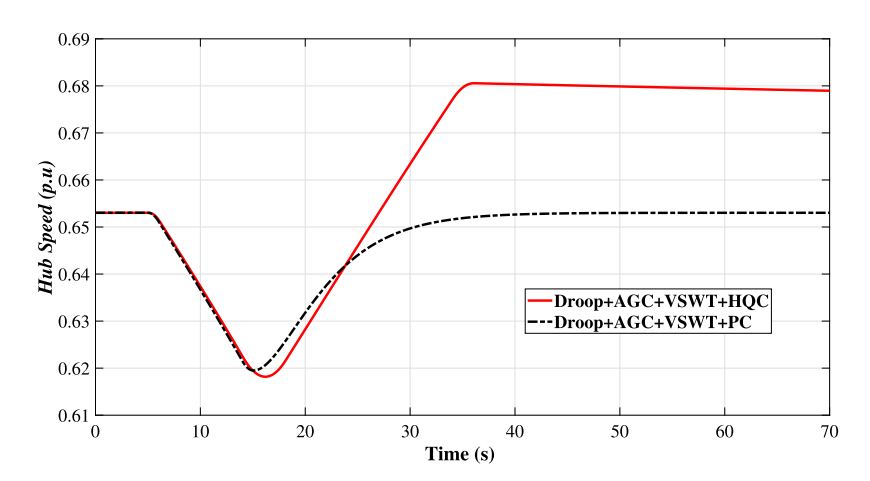


Fig. 14. Wind turbine hub speed in the Hydro-Quebec and the proposed algorithms.

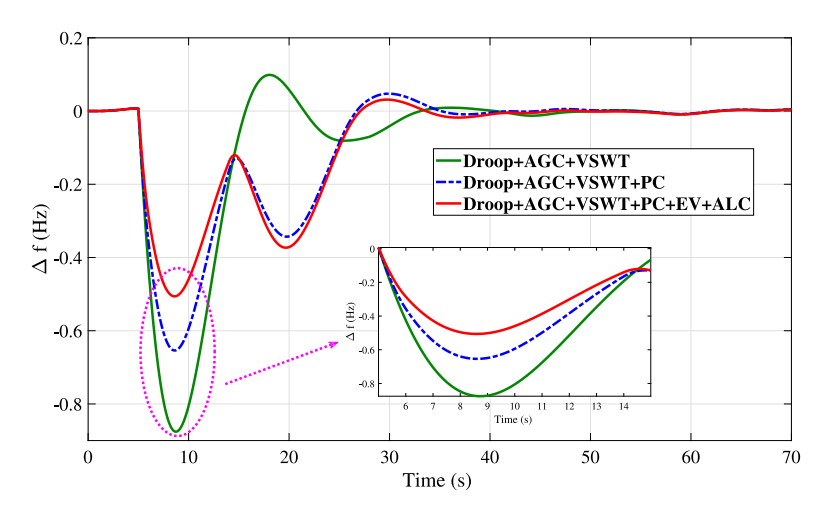


Fig. 15. Power system frequency response considering VSWT, proposed controller, EV and ALC.

of second frequency dip decreases significantly. To reduce the effect of the communication delay on EVs participation to control the second frequency dip, the ALC is attached to the second state and is considered as the third state. The frequency fluctuation is depicted by the solid green curve in Fig. 16. The amount of second frequency dip drops which shows the importance of EVs

activation at an appropriate moment and the efficiency of the proposed ALC.

6. Comparison to similar studies

At this point, the outcomes of this study are compared to the findings of other research works to demonstrate the efficacy of the

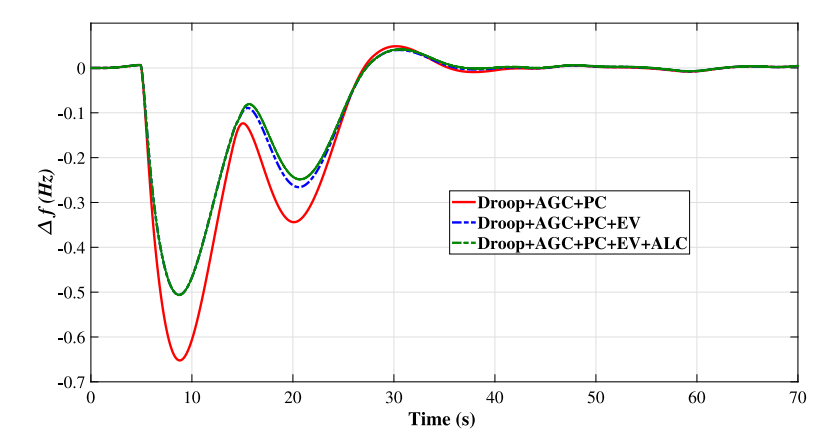


Fig. 16. Alleviating of the second frequency dip by employing another group of EVs and ALC at an appropriate moment.

suggested algorithms and controllers connected to employing EV and VSWTs to improve the power system frequency regulation.

Comparison of the results presented in Sections 2 and 3 with the findings of Ref. [20]:

In Ref. [20], a new V2G method was proposed for grid frequency control in the presence of EVs in a smart deregulated electricity system. To collaborate with EVs in power system frequency regulation, enhanced fuzzy logic controllers have been adopted. Fuzzy controllers took into account the SOC of the batteries and the grid frequency deviation as two input variables. The charge or discharge power of EV batteries was calculated with regard to these inputs, taking into account membership functions as well as fuzzy rules.

The proposed methods in Ref. [20] have been implemented in the modified IEEE39-bus test power system, the test system of this paper. Here, the proposed methods and controllers in Sections 2 and 3 and Ref. [20] for evaluating EVs' participation in the power system frequency regulation have been utilized. In this scenario, at t = 5 s, a step load increment of $\Delta P_L = 175$ MW is applied in the system as a disturbance. At first state, the EV with the proposed virtual inertia controller mentioned in Section 2 is added to the power system. The disturbance is applied and the frequency excursion is depicted in Fig. 17 with the dashed blue curve. In the second state, the algorithms and methods described in Ref. [20] have been put into practice. The frequency fluctuation in the face of a similar disturbance is shown in Fig. 17 with the solid green curve. Although the second state's findings have a slightly shorter settling time than the first state, the first state's nadir frequency is noticeably better than the second state's which demonstrates the superiority of the suggested strategy in Section 2 of this paper. Finally, in the third state, the ALC with $\tau = 400 \text{ ms}$ is attached to the virtual inertia controller, the first state, to decrease the effect of communication latency. The frequency excursion of this state is sketched in Fig. 17 with the solid red curve. In comparison to the other states, the frequency deviation and nadir frequency amount have improved which shows the performance of the proposed algorithms and controllers related to EV and ALC in Sections 2 and 3.

• Comparison of the results presented in Section 4 with the findings of Ref. [33]:

Ref. [33] presents novel controllers for wind turbines based on doubly fed induction generators (DFIG). These controllers not only optimize the transient behavior of DFIGs, but also actualize their involvement in the frequency control duty of the power system. One primary speed controller and two auxiliary controllers are offered as controllers. To provide the best transient response, the main speed controller is a fuzzy-based controller whose parameters are tuned using the genetic algorithm (GA). It uses the

rotational speed signal to cause the DFIG to swiftly return to the maximum power point (MPP) following any turbulent changes in wind speed. Furthermore, two smart auxiliary controllers are proposed: frequency deviation and wind speed oscillations controllers. The frequency deviation controller offers DFIG frequency support, whilst the wind speed oscillations controller mitigates the effects of wind speed changes on wind turbine output power by utilizing wind turbine kinetic energy.

The proposed methods in Ref. [33] have been implemented in the modified IEEE39-bus test power system, the test system of this paper. At this point, the proposed algorithms and controllers in Section 4 and Ref. [33] for evaluating VSWTs' participation in the power system frequency regulation have been utilized. In this scenario, around 40% of the power is provided by wind farms to support frequency control. Furthermore, at t = 5 s, a step load increment $\Delta P_L = 175$ MW is applied in the system as a disturbance. Here, there are three states. The first state includes conventional and wind power plants considering the proposed Hydro-Quebec controller for wind turbines. In the second state, the proposed controller in Section 4.2 is replaced by the Hydro-Quebec controller. In the third state, the proposed controllers in the Ref. [33] are applied to the power system and manage VSWTs to collaborate in the power system frequency regulation. After occurring the disturbance, at the first state, the frequency excursion is depicted in Fig. 18 by the solid red curve. When the proposed controller of this paper is added to the VSWT, the frequency response is shown by the dashed black curve in Fig. 18. The nadir frequency improves greatly in this situation because VSWTs can collaborate more to recover frequency based on the value of 'M'. Finally, at the third state, the proposed controller in Ref. [33] is considered in the VSWT and the frequency pattern is shown by the solid blue curve in Fig. 18. The nadir and settling time of the frequency fluctuation are improved remarkably compared to the proposed controller in Ref. [33] which shows the effectiveness of the proposed algorithms.

7. Conclusion

In this paper, to realize further improvement in the power system frequency response in presence of wind power plants, the electric vehicle (EV) and variable speed wind turbine (VSWT) were added to the power system. Based on the IEC 61851 standard, the virtual inertia controller containing the modification phase for avoiding EV output current oscillation was proposed for EV collaboration in the power system frequency. To increase the effectiveness of the EV in the frequency control, an adaptive latency controller (ALC) was proposed to decrease the effect of communication latency. To extract the ability of VSWT in frequency adjustment, an algorithm was proposed. In that algorithm, in

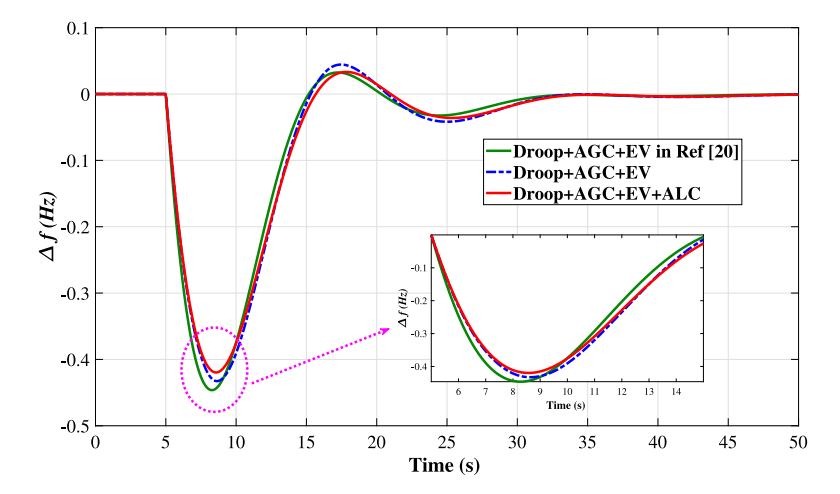


Fig. 17. Comparison between the frequency response using the proposed methods in Sections 2 and 3 and methods applied in Ref. [20].

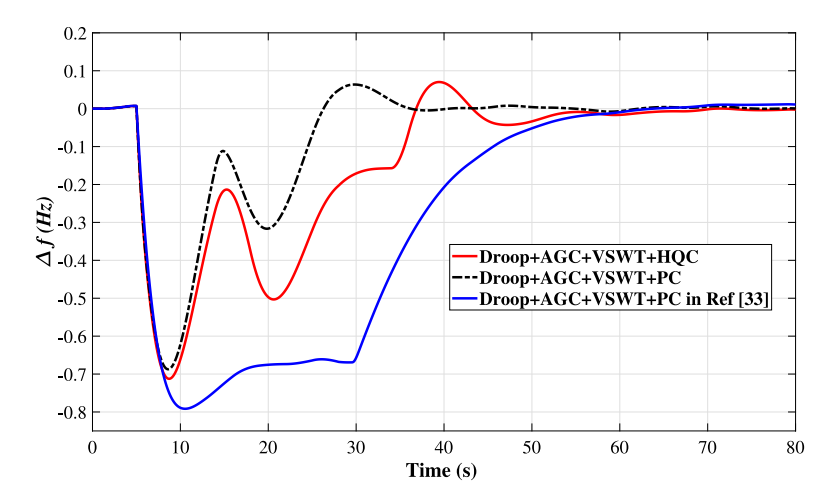


Fig. 18. Comparison between the frequency response using the proposed methods in Section 4 and methods applied in Ref. [33].

face of disturbances, the VSWT output power is increased in one second to the maximum allowable value and will be fixed. Notice, another algorithm for finding the maximum increment power was presented. After operating in the uniform support state for 10 s or when the VSWT hub speed reaches lower than minimum acceptable hub speed, ω_{\min} , the VSWT will be recovered. Two PID controllers were designed for operating in support and recovery zones. The proposed algorithms were applied to the modified IEEE 39-bus test power system and the results confirmed the superiority of the suggested methods. Applying the EV and the VSWT in the power system separately enhances the frequency response. The most efficient way to improve the system frequency behavior was obtained when both EV with the designed ALC and the proposed algorithm in VSWT were utilized simultaneously.

CRediT authorship contribution statement

Seyed Amir Hosseini: Conceptualization, Software, Validation, Formal analysis, Writing – original draft, Methodology, Data curation, Investigation, Visualization, Writing – review.

Declaration of competing interest

All authors have participated in (a) conception and design, or analysis and interpretation of the data; (b) drafting the article or revising it critically for important intellectual content; and (c) approval of the final version.

This manuscript has not been submitted to, nor is under review at, another journal or other publishing venue.

The authors have no affiliation with any organization with a direct or indirect financial interest in the subject matter discussed in the manuscript

Data availability

No data was used for the research described in the article.

References

- [1] Toulabi M, Bahrami S, Ranjbar AM. An input-to-state stability approach to inertial frequency response analysis of doubly-fed induction generator-based wind turbines. IEEE Trans Energy Convers 2017;32(4):1418–31.
- [2] Hosseini SA, Toulabi M, Ashouri-Zadeh A, Ranjbar AM. Modified power reserve management solution in power system considering frequency constraints. IEEE Syst J 2019;14(1):1125–34.
- [3] Muljadi E, Gevorgian V, Singh M, Santoso S. Understanding inertial and frequency response of wind power plants. IEEE; 2012.
- [4] Zografos D. Power system inertia estimation and frequency response assessment (Ph.D. thesis), KTH Royal Institute of Technology; 2019.
- [5] Adrees A, Papadopoulos P, Milanovic J. A framework to assess the effect of reduction in inertia on system frequency response. In: 2016 IEEE power and energy society general meeting (PESGM). IEEE; 2016, p. 1–5.
- [6] Hosseini SA, Toulabi M, Dobakhshari A, Ashouri-Zadeh A, Ranjbar AM. Delay compensation of demand response and adaptive disturbance rejection applied to power system frequency control. IEEE Trans Power Syst 2019;35(3):2037–46.
- [7] Strbac G. Demand side management: Benefits and challenges. Energy Policy 2008;36(12):4419–26.

- [8] Shi Q, Li F, Hu Q, Wang Z. Dynamic demand control for system frequency regulation: Concept review, algorithm comparison, and future vision. Electr Power Syst Res 2018;154:75–87.
- [9] Nayak A, Rana R, Mishra S. Frequency regulation by electric vehicle during grid restoration using adaptive optimal control. IFAC-PapersOnLine 2019;52(4):270–5.
- [10] Rahman T, Qu Z. The role of electric vehicles for frequency regulation during grid restoration. In: 2017 IEEE power & energy society general meeting. IEEE; 2017, p. 1–5.
- [11] Luo Z, Hu Z, Song Y, Xu Z, Lu H. Optimal coordination of plug-in electric vehicles in power grids with cost-benefit analysis—Part I: Enabling techniques. IEEE Trans Power Syst 2013;28(4):3546–55.
- [12] Rogers K, Klump R, Khurana H, Aquino-Lugo A, Overbye T. An authenticated control framework for distributed voltage support on the smart grid. IEEE Trans Smart Grid 2010;1(1):40–7.
- [13] Zhao J, Wan C, Xu Z, Wong K. Spinning reserve requirement optimization considering integration of plug-in electric vehicles. IEEE Trans Smart Grid 2016;8(4):2009–21.
- [14] Liu H, Huang K, Wang N, Qi J, Wu Q, Ma S, Li C. Optimal dispatch for participation of electric vehicles in frequency regulation based on area control error and area regulation requirement. Appl Energy 2019;240:46–55.
- [15] Elsisi M, Soliman M, Aboelela M, Mansour W. Model predictive control of plugin hybrid electric vehicles for frequency regulation in a smart grid. IET Gener Transm Distrib 2017;11(16):3974–83.
- [16] Han S, Han S, Sezaki K. Design of an optimal aggregator for vehicle-to-grid regulation service. In: 2010 innovative smart grid technologies (ISGT). IEEE; 2010, p. 1–8.
- [17] Meng J, Mu Y, Jia H, Wu J, Yu X, Qu B. Dynamic frequency response from electric vehicles considering travelling behavior in the great britain power system. Appl Energy 2016;162:966–79.
- [18] Liu H, Hu Z, Song Y, Lin J. Decentralized vehicle-to-grid control for primary frequency regulation considering charging demands. IEEE Trans Power Syst 2013;28(3):3480–9.
- [19] Ota Y, Taniguchi H, Nakajima T, Liyanage K, Baba J, Yokoyama A. Autonomous distributed V2G (vehicle-to-grid) satisfying scheduled charging. IEEE Trans Smart Grid 2011;3(1):559–64.
- [20] Falahati S, Taher SA, Shahidehpour M. Grid frequency control with electric vehicles by using of an optimized fuzzy controller. Appl Energy 2016:178:918–28.
- [21] Khooban M. Secondary load frequency control of time-delay stand-alone microgrids with electric vehicles. IEEE Trans Ind Electron 2017;65(9):7416–22.

- [22] Mu C, Liu W, Xu W. Hierarchically adaptive frequency control for an EV-integrated smart grid with renewable energy. IEEE Trans Ind Inf 2018;14(9):4254–63.
- [23] Hansen A, Altin M, Iov F. Provision of enhanced ancillary services from wind power plants-examples and challenges. Renewable Energy 2016;97:8–18.
- [24] Kheshti M, Ding L, Bao W, Yin M, Wu Q, Terzija V. Toward intelligent inertial frequency participation of wind farms for the grid frequency control. IEEE Trans Ind Inf 2019;16(11):6772–86.
- [25] Morren J, Pierik J, De Haan S. Inertial response of variable speed wind turbines. Electr Power Syst Res 2006;76(11):980-7.
- [26] Tarnowski G, Kjar P, Sorensen P, Ostergaard J. Variable speed wind turbines capability for temporary over-production. In: 2009 IEEE power & energy society general meeting. IEEE; 2009, p. 1–7.
- [27] Ebrahimi M, Khajehoddin SA, Karimi-Ghartemani M. An improved damping method for virtual synchronous machines. IEEE Trans Sustain Energy 2019;10(3):1491–500.
- [28] Du W, Fu Q, Wang H. Power system small-signal angular stability affected by virtual synchronous generators. IEEE Trans Power Syst 2019;34(4):3209–19.
- [29] Alipoor J, Miura Y, Ise T. Stability assessment and optimization methods for microgrid with multiple VSG units. IEEE Trans Smart Grid 2016;9(2):1462–71.
- [30] Brisebois J, Aubut N. Wind farm inertia emulation to fulfill hydro-québec's specific need. In: 2011 IEEE power and energy society general meeting. IEEE; 2011, p. 1–7.
- [31] Ghosh S, Kamalasadan S, Senroy N, Enslin J. Doubly fed induction generator (DFIG)-based wind farm control framework for primary frequency and inertial response application. IEEE Trans Power Syst 2015;31(3):1861–71.
- [32] Ramtharan G, Jenkins N, Ekanayake J. Frequency support from doubly fed induction generator wind turbines. IET Renew Power Gener 2007;1(1):3-9.
- [33] Ashouri-Zadeh A, Toulabi M, Ranjbar AM. Coordinated design of fuzzy-based speed controller and auxiliary controllers in a variable speed wind turbine to enhance frequency control. IET Renew Power Gener 2016;10(9):1298–308.
- [34] Commission IE. Electric vehicle conductive charging system-part 1: General requirements. IEC Stand 2017;61851-1.
- [35] Naduvathuparambil B, Valenti M, Feliachi A. Communication delays in wide area measurement systems. In: Proc. southeastern symp. syst. theory. Huntsville, AL, USA.; 2002, p. 118–22.
- [36] Silva GJ, Datta A, Bhattacharyya SP. New results on the synthesis of PID controllers. IEEE Trans Automat Control 2002;47(2):241–52.
- [37] Slootweg J, Polinder H, Kling W. Representing wind turbine electrical generating systems in fundamental frequency simulations. IEEE Trans Energy Convers 2003;18(4):516–24.
- [38] [link]. URL https://www.dropbox.com/s/3upke27u2bi6ssz/data.xlsx?dl=0.